

# Magnetic Resonance Imaging: Principles and Techniques: Lessons for Clinicians

Vijay P.B. Grover<sup>\*</sup>, Joshua M. Tognarelli<sup>\*</sup>, Mary M.E. Crossey<sup>\*</sup>, I. Jane Cox<sup>†</sup>,  
Simon D. Taylor-Robinson<sup>\*</sup>, Mark J.W. McPhail<sup>\*</sup>

<sup>\*</sup>Liver Unit, Division of Diabetes, Endocrinology and Metabolism, Department of Medicine, Imperial College London, London, United Kingdom and  
<sup>†</sup>Institute of Hepatology, University of London, Chenies Mews, Fitzrovia, London, United Kingdom

**The development of magnetic resonance imaging (MRI) for use in medical investigation has provided a huge forward leap in the field of diagnosis, particularly with avoidance of exposure to potentially dangerous ionizing radiation. With decreasing costs and better availability, the use of MRI is becoming ever more pervasive throughout clinical practice. Understanding the principles underlying this imaging modality and its multiple applications can be used to appreciate the benefits and limitations of its use, further informing clinical decision-making. In this article, the principles of MRI are reviewed, with further discussion of specific clinical applications such as parallel, diffusion-weighted, and magnetization transfer imaging. MR spectroscopy is also considered, with an overview of key metabolites and how they may be interpreted. Finally, a brief view on how the use of MRI will change over the coming years is presented. (J CLIN EXP HEPATOL 2015;5:246–255)**

**T**he nuclear magnetic resonance (NMR) phenomenon was first described experimentally by both Bloch and Purcell in 1946, for which they were both awarded the Nobel Prize for Physics in 1952.<sup>1,2</sup> The technique has rapidly evolved since then, following the introduction of wide-bore superconducting magnets (approximately 30 years ago), allowing development of clinical applications. The first clinical magnetic resonance images were produced in Nottingham and Aberdeen in 1980, and magnetic resonance imaging (MRI) is now a widely available, powerful clinical tool.<sup>3,4</sup> This article covers a brief synopsis of basic principles in MRI, followed by an overview of current applications in medical practice.

All atomic nuclei consist of protons and neutrons, with a net positive charge. Certain atomic nuclei, such as the hydrogen nucleus, <sup>1</sup>H, or the phosphorus nucleus, <sup>31</sup>P, possess a property known as “spin”, dependent on the number of protons. This can be conceived as the nucleus spinning around its own axis although this is a mathematical analogy. The nucleus itself does not spin in the

classical meaning but by virtue of its constituent parts induces a magnetic moment, generating a local magnetic field with north and south poles. The quantum mechanical description of this dipolar magnet is analogous to classical mechanics of spinning objects. The dipole itself is analogous to a bar magnet, with magnetic poles aligning along its axis of rotation (Figure 1).<sup>5</sup>

Application of a strong, external magnetic field ( $B_0$ ) aligns the nucleus either in parallel with or perpendicular to the external field. A liquid solution containing many nuclear spins, placed within the  $B_0$  field, will contain nuclear spins in one of two energy states: a low-energy state (oriented parallel to the magnetic field) or a high-energy state (orientated perpendicular to the magnetic field direction). In solids or liquids, there would tend to be an excess of spins in the same direction as  $B_0$ . Although a bar magnet would orientate completely parallel or antiparallel to the field, the nucleus has an angular momentum due to its rotation, so it will rotate, or precess, around the  $B_0$  axis (Figure 2). This behavior is often compared to the wobbling motion of a gyroscope under the influence of the Earth’s magnetic field and explains the use of “spin” to explain what is in reality a quantum mechanical phenomenon. The velocity of rotation around the field direction is the Larmor frequency. This is proportional to the field strength, and is described by the Larmor equation (Figure 3).<sup>5</sup>

Nuclei that possess spin can be excited within the static magnetic field,  $B_0$ , by application of a second radiofrequency (RF) magnetic field  $B_1$ , applied perpendicular to  $B_0$ . The RF energy is usually applied in short pulses, each lasting microseconds. The absorption of energy by the nucleus causes a transition from higher to lower energy levels and vice versa on relaxation. The energy absorbed (and subsequently emitted) by the nuclei induces a voltage that can be detected by a suitably tuned coil of wire,

*Keywords:* magnetic resonance imaging, magnetic resonance spectroscopy, nuclear magnetic resonance, medical physics, nuclear medicine

*Received:* 31.07.2015; *Accepted:* 10.08.2015; *Available online:* 20 August 2015

*Address for correspondence:* Joshua Tognarelli, Liver Unit, Department of Medicine, 10th Floor QEOM Wing, St Mary’s Hospital, Imperial College London, Praed Street, London W2 1NY, United Kingdom.

*Tel.:* +44 207 886 6454; *fax:* +44 207 402 2796.

*E-mail:* jt2110@imperial.ac.uk

*Abbreviations:* ADC: apparent diffusion coefficient; CSI: Chemical shift imaging; DTI: diffusion tensor imaging; DWI: Diffusion-weighted imaging; FA: Fractional anisotropy; FID: free induction decay; MRI: magnetic resonance imaging; MTR: MT ratios; NMR: nuclear magnetic resonance; PRESS: Point-resolved spectroscopy; RA: relative anisotropy; RF: radiofrequency; SNR: signal-to-noise ratio; STEAM: Stimulated echo acquisition mode; TR: repetition time

<http://dx.doi.org/10.1016/j.jceh.2015.08.001>

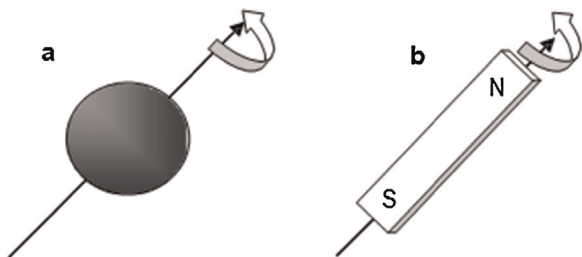


**Figure 1** Nuclear spin. The “spinning” nucleus (a) induces a magnetic field, behaving like a bar magnet (b). N and S represent north and south respectively. The directions of the arrows represent the direction of the magnetic field.

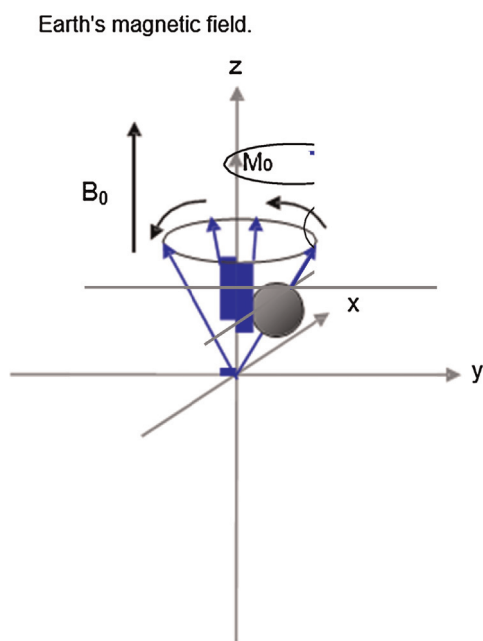


**Figure 2** Nucleus precessing around an external magnetic field ( $B_0$ ).  $M_0$  = direction of net magnetization.  $x$ ,  $y$  and  $z$  represent the orthogonal Cartesian axes.  $\omega_0 = \gamma B_0$

amplified and displayed as the “free-induction decay” (FID). In the absence of continued RF pulsation, relaxation processes will return the system to thermal equilibrium. Therefore, each nucleus will resonate at a characteristic frequency when placed within the same magnetic field.<sup>5</sup>

The energy required to induce transition between energy levels is the energy difference between the two nuclear spin states. This depends on the strength of the  $B_0$  magnetic field the nuclei are subjected to (Figure 4). Application of an RF pulse at the resonant frequency generates a FID. In practice, multiple RF pulses are applied

$$\omega_0 = \gamma B_0$$

**Figure 3 Larmor equation.**  $\omega_0$  = angular frequency of the protons,  $\gamma$  is the gyromagnetic ratio, a constant fixed for a specific nucleus and  $B_0$  is the field strength.  $\Delta E = \gamma h B_0 / 2\pi$

$$\Delta E = \gamma h B_0 / 2\pi!$$

**Figure 4** Difference in energies of the two spin orientations, where  $h$  = Planck’s constant.

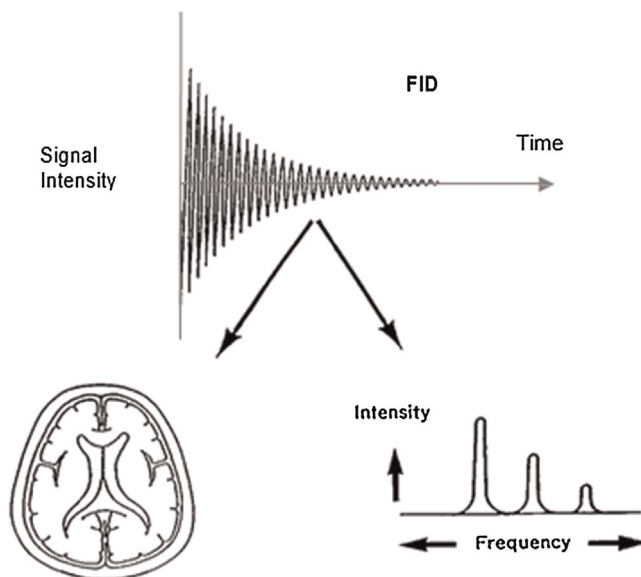


**Figure 5** The free induction decay (FID) and Fourier transformation to generate MR images or MR spectra.

to obtain multiple FIDs, which are then averaged to improve the signal-to-noise ratio (SNR). The signal-averaged FID is a time-domain signal. It will be made up of contributions from different nuclei within the environment being studied (e.g. free water and  $^1H$  bound to tissue). The signal-averaged FID can be resolved by a mathematical process known as Fourier transformation, into either an image (MRI) or a frequency spectrum, providing biochemical information (Figure 5).<sup>5</sup>

### MR FIELD GRADIENTS

Localizing the MR signal spatially to a region of interest requires the use of gradients. These are additional spatially linear variations in the static field strength. Gradients can be applied in any orthogonal direction using the three sets of gradient coils,  $G_x$ ,  $G_y$ , and  $G_z$ , within the MR system. Faster or slower precession is detected as higher or lower MR signal. Thus, the frequency measurements can be used to distinguish MR signals at different positions in space and enable image reconstruction in three dimensions (Figure 6).<sup>5</sup>

### RF COILS

The transmitter and receiver coils may be either separate or individual pieces of hardware, depending on the area of body under examination and the experiment being

MRI

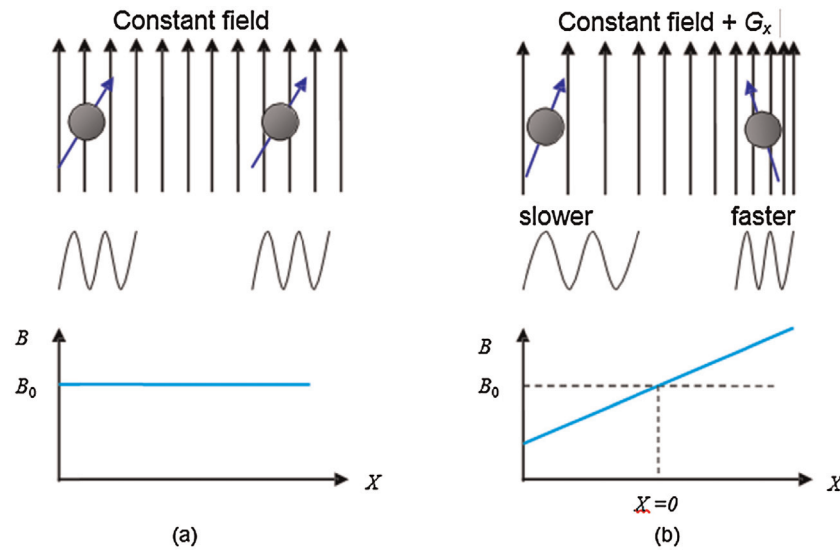


**Figure 6** Effect of field gradient on nuclei.

(a)  $B_0$  only, all nuclei precess at the same frequency.

(b)  $B_0$  with gradient  $G_x$ . Further along the  $x$  direction the field increases and thus the protons resonate faster- precession frequency depends upon position.

Adapted from McRobbie, D et al. *MRI From Picture to Proton*. 1st edn. Cambridge. Cambridge University Press, 2003. MTR + 100 × (SI off – SI on)/SI

performed. The applied  $B_1$  pulse is applied by an enveloping transmitter coil, which uniformly surrounds the area of interest, such as a head coil. The receiver coil consists of a loop of wire, which may either be placed directly over the region of interest or combined within the transmitter coil. Phased-array coils involve a number of coils receiving MR signal simultaneously and independently from a single excitation. If each coil is connected to a separate receiver, then the noise between the coils is uncorrelated, resulting in a higher signal-to-noise ratio than if the coils were just connected to one receiver. Mathematical algorithms can then be employed to combine the data from the individual coils to generate an optimum reconstructed image.<sup>5</sup>

## PARALLEL IMAGING

Parallel imaging is an MR technique designed to reduce scan time. Sensitivity encoding (SENSE<sup>TM</sup>, Philips) and simultaneous acquisition of spatial harmonics (SMASH) are two such examples. SENSE works through under-sampling of the MR data and by collecting data simultaneously from multiple imaging coils. Reconstruction of the data requires an accurate knowledge of the individual coil sensitivities prior to the acquisition of the data. Therefore, a reference scan acquiring low resolution individual coil data is acquired prior to the main imaging sequence. Thus, a SENSE factor of 2 may reduce imaging time by up to 50%. However, with higher SENSE factors there may be a diminishing amount of MR signal that is recorded.<sup>5</sup>

## THE MRI SCANNER

Current diagnostic MRI scanners use cryogenic superconducting magnets in the range of 0.5 Tesla (T) to 1.5 T. By comparison, the Earth's magnetic field is 0.5 Gauss (G), which is equivalent to 0.00005 T. Cooling the magnet to a temperature close to absolute zero (0 K) allows such huge currents to be conducted; this is most commonly performed via immersion in liquid helium. Until recently, most clinical research was conducted at a field strength of 1.5 T. However, 3 T systems are now widely available and are being used regularly in the research setting, where the capabilities of 3 T systems are being explored and optimized. The advantages of higher field strength systems include improved signal-to-noise ratio (SNR), higher spectral, spatial, and temporal resolution, and improved quantification. The improved SNR can be traded to allow a reduced imaging time. Inherent disadvantages include magnetic susceptibility, eddy current artifacts, and magnetic field instability.<sup>6,7</sup>

Magnetic susceptibility is the degree of magnetization that a tissue or material exhibits in response to a magnetic field. This may have either a beneficial or deleterious effect on the overall image quality. Magnetic susceptibility artifacts are more prominent at 3 T compared to 1.5 T. The phenomenon may be beneficial in functional or diffusion MRI by improving tissue contrasts, but disadvantageous by producing signal voids at air/tissue interfaces in diffusion sequences. An eddy current is an induced current generated due to the interaction between the rapidly

changing magnet field and the conducting structures within the MRI scanner. Eddy currents may lead to perturbations in the gradient field, reducing resolution of the subsequent MR Image.<sup>7</sup>

### T1- AND T2-WEIGHTED MR IMAGING

Relaxation is the term used to describe the process by which a nuclear “spin” returns to thermal equilibrium after absorbing RF energy. There are two types of relaxation, longitudinal and transverse relaxations, and these are described by the time constants,  $T_1$  and  $T_2$ , respectively.<sup>5</sup>

$T_1$  is also known as “spin-lattice relaxation”, whereby the “lattice” is the surrounding nucleus environment. As longitudinal relaxation occurs, energy is dissipated into the lattice.  $T_1$  is the length of time taken for the system to return 63% toward thermal equilibrium following an RF pulse as an exponential function of time.  $T_1$  can be manipulated by varying the times between RF pulses, the repetition time (TR). Water and cerebrospinal fluid (CSF) have long  $T_1$  values (3000–5000 ms), and thus they appear dark on  $T_1$ -weighted images, while fat has a short  $T_1$  value (260 ms) and appears bright on  $T_1$ -weighted images.<sup>5</sup>

Relaxation processes may also redistribute energy among the nuclei within a spin system, without the whole spin system losing energy. Thus, when a RF pulse is applied, nuclei align predominantly along the axis of the applied energy. On relaxation, there is dephasing of nuclei orientations as energy is transferred between the nuclei and there is reduction in the resultant field direction, with a more random arrangement of alignments. This is  $T_2$ , termed transverse relaxation, because it is a measure of how fast the spins exchange energy in the “xy” plane.  $T_2$  is also known as “spin-spin” relaxation.<sup>5</sup>

### MAGNETIZATION TRANSFER IMAGING (MT)

MT indirectly allows measurement of bound and free water compartments in the brain. It can be affected by variations in membrane fluidity, heavy metal concentration, and total water content.<sup>8,9</sup> MT itself is a technique for manipulating tissue contrast.<sup>10,11</sup> In addition to enabling acquisition of images with enhanced contrast, techniques employing MT allow measurement of MT ratios (MTR) (Figure 7). MTR is a quantitative tissue characteristic reflecting the behavior of normally MR-invisible protons bound to macromolecules. MTR measurement can detect

$$\text{MTR} = 100 \times (\text{SI off} - \text{SI on}) / \text{SI}$$

**Figure 7 MTR formula.** (SI off = signal intensity in the baseline proton density image, SI on = signal intensity in the image with the MT pulse applied).

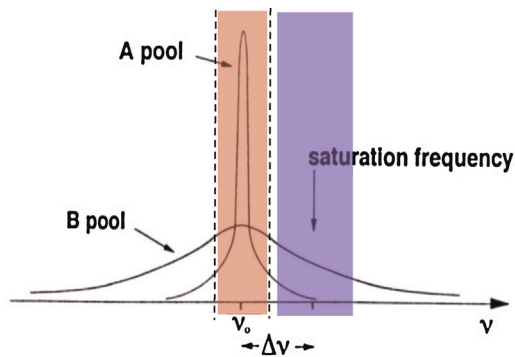


**Figure 8** Model demonstrating the concepts underlying the phenomenon of magnetization transfer.

parenchymal changes in the brain that may not be seen using standard MR techniques.<sup>5</sup> In essence, protons in tissues exist in two pools, free and bound. Mobile protons, such as those found in body water make up the free pool; it has a narrow spectral line with relatively long  $T_1$  and  $T_2$  relaxation times (Figure 8). The majority of signal in conventional MR applications comes from the free pool, as the range for MR excitation frequency is narrow and centered on these mobile protons. A second pool of protons bound in proteins and other macromolecules or membranes is referred to as being MR invisible, as it is not typically within the excitation frequency range used. This pool has a much broader spectral line and shorter relaxation times, giving a lower SNR (Figure 8). Magnetization can be transferred between pools bidirectionally through direct interaction between spins, transfer of nuclei or direct chemical means. Under normal circumstances, magnetization transfer is the same in both directions.<sup>5</sup>

Techniques employing MT saturate the magnetization in the bound pool, leaving the free pool mostly unaffected. This is possible due to the broad spectral line of the bound pool. It can be excited through the use of an “off-resonance” RF pulse (Figure 8). The saturation of the bound pool causes substantial attenuation of the magnetization. Consequently, there is little transfer of the magnetization to the free pool, with the effective longitudinal magnetization within it and its  $T_1$  relaxation time reduced as a consequence. Pulse sequences incorporating the use of “off-resonance” pulses can be designed to quantitate the effect of MT in different tissues.<sup>10</sup>

The free pool of protons (A) has a narrow spectral line, resonating at the Larmor frequency ( $\nu_0$ ). RF pulses covering the frequencies, which are shown in pink (Figure 8), are able to excite the free pool. The “bound” pool (B) has a broad spectral line, while the subsequent application of RF irradiation at a frequency offset by  $\Delta\nu$ , shown in blue, can excite and saturate the pool without significantly affecting the free pool (pool A).

MRI



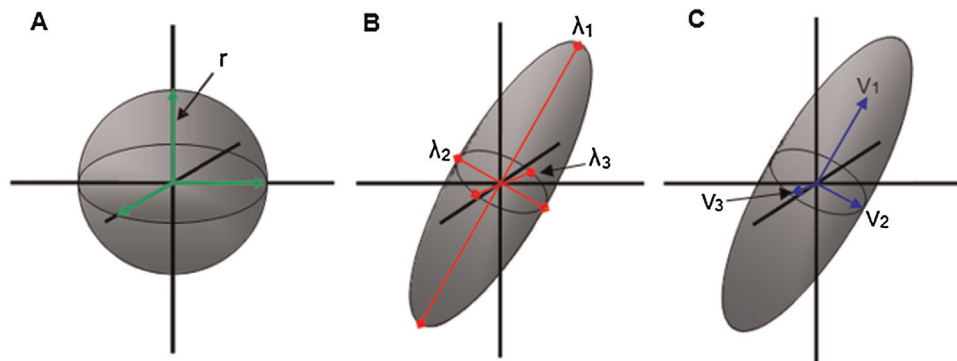


**Figure 9 Principles of diffusion.** Isotropic (A) diffusion and restricted diffusion (B and C). See text for further explanation.

## DIFFUSION-WEIGHTED IMAGING

Diffusion-weighted imaging (DWI) is an MR technique allowing quantification of water molecule movement. In the early 1990s, DWI was pioneered to detect acute cerebral ischemia.<sup>12,13</sup> Other indications include investigation for multiple sclerosis and brain tumors.<sup>14–16</sup>

Water molecule diffusion follows the principles of Brownian motion. Thus, when unconstrained, water molecule movement is random and equal in all directions. This random movement is described as “isotropic”. However, motion of water molecules in structured environments is restricted due to their physical surroundings. In the brain, the microstructure within gray and white matter restricts water molecule movement. On average, water molecules tend to move parallel to white matter tracts, as opposed to perpendicular to them.<sup>17,18</sup> This motion is described as “anisotropic”, as it is not equal in all directions. The molecules’ motion in the  $x$ ,  $y$  and  $z$  planes and the correlation between these directions is described by a mathematical construct, known as the diffusion tensor.<sup>19,20</sup> In mathematics, a tensor defines the properties of a three-dimensional ellipsoid. For the diffusion tensor to be determined, diffusion data in a minimum of six noncollinear directions are required. This process is known as diffusion tensor imaging (DTI). **Figure 9** shows the graphical representation of a diffusion tensor, as a three-dimensional ellipsoid; the long axis represents the primary direction of motion.<sup>20</sup>

Unconstrained, a water molecule would move randomly and equally in all directions, isotropic diffusion (A). The radius “ $r$ ” of the spherical range of motion seen in **Figure 9** defines the probability of motion in a given direction. Anisotropic diffusion will occur in an ordered environment, for example within the white matter, and will form an elliptical range of motion (B and C). Three eigenvalues,  $\lambda_1$ ,  $\lambda_2$ , and  $\lambda_3$  and three eigenvectors  $v_1$ ,  $v_2$  and  $v_3$  define the shape and orientation of the ellipsoid, respectively (**Figure 9**), describing the magnitude and directions of the three major planes of the diffusion ellipsoid.<sup>21</sup> During

DTI, the tensor is calculated at each pixel location, allowing a map of diffusion to be produced, showing the magnitude and dominant direction of the process. When followed across a number of pixels, the dominant directions plot lines along which diffusion is most likely to occur. Practicing this technique is known as tractography, due to the theory that the likely diffusion of these paths represents the white matter tracts.

## APPARENT DIFFUSION COEFFICIENT

DTI collects detailed information allowing insight into the microstructure found within an imaging voxel. Factors calculated include the mean diffusivity, degree of anisotropy, and direction of the diffusivities.<sup>22</sup> Mean diffusivity is a measure of displacement of water and also the presence of obstacles to movement at a cellular and subcellular level. Using differently weighted DWI images, a measure of diffusion can be calculated. The different images can be mapped to create an apparent diffusion coefficient (ADC) Image.<sup>23</sup> The ADC measures tissue water diffusivity dependent on the interactions between water molecules and their surrounding structural and chemical environment.<sup>24</sup>

## FRACTIONAL ANISOTROPY

Fractional anisotropy (FA) and relative anisotropy (RA) are terms frequently used to describe the degree of anisotropy. Anisotropy relates to physical barriers, affected by characteristics, such as the density, orientation, size, and shape of nerve fibers within white matter tracts. However, myelination has been demonstrated not to be an essential component for anisotropy, though it certainly does contribute to the development of it, with nonmyelinated nerves also having the potential to exhibit anisotropy.<sup>25</sup> The direction of the anisotropy, and therefore the fibers, can be plotted on color-coded two-dimensional maps (**Figure 10**), or otherwise by three-dimensional tractography. Various algorithms can be used to calculate the orientation of

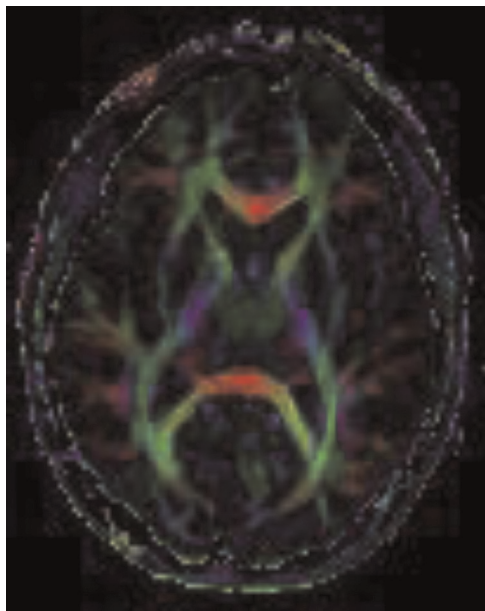


**Figure 10 Color fractional anisotropy (FA) image from a 44-year-old healthy male volunteer.** Diffusion tensor imaging (DTI) imaging performed on a 3 T Philips Intera™ using 32 different directions of diffusion sensitization. The different colors represent the principle diffusion directions and hence the direction of the white matter tracts: green represents anterior-posterior, blue represents caudo-cranial, red represents transverse.

the major axonal fiber bundles using eigenvectors and eigenvalues.<sup>21</sup> Three-dimensional expression of DTI data is one of the latest developments using this technique and may provide a better understanding into failings in brain connectivity.

## MR FIELD STRENGTH

Clinical imaging at 3 T field strength instead of 1.5 T has advantages in diffusion-weighted imaging. The advantages are improved signal-to-noise ratio by 30–50%, improved contrast-to-noise ratio by up to 96% and reduced variability in ADC and FA by 34–52%.<sup>26–28</sup> Disadvantages of imaging at 3 T include susceptibility artifact and image distortion; but this can be attenuated significantly by parallel imaging techniques, such as SENSE™ (sensitivity encoding).<sup>26,28,29</sup> Field strength should make no difference to the values of FA and ADC obtained, but should improve the accuracy and precision of those measurements.<sup>26,28,30</sup>

## NUMBER OF DIFFUSION DIRECTIONS

Cellular structures are not orientated in perfect symmetrical alignment homogeneously throughout the body, and thus the measurement of the diffusion of water molecules will be directionally dependent. This means that diffusion needs to be measured in several directions to obtain a rotationally invariant estimate of isotropic diffusion.

Various experiments and modeling strategies have been employed to determine the minimal number of diffusion directions required to obtain an isotropic voxel, from which robust ADC and FA data can be derived, thus allowing a reasonable scan time for the patient with acquisition of reliable data. The minimal number of directions is reported as 20–30,<sup>31,32</sup> although ADCs can be calculated with a minimum of 6 noncollinear directions. Diffusion weighting is expressed as a  $b$  value, which is dependent on the characteristics of the MR sequence. The  $b$  value increases with increasing diffusion weighting, and sufficient diffusion weighting is usually achieved with a  $b$  value of 1000 s/mm<sup>2</sup>. Two-point ADC estimates, with  $b_0$  and 1000 s/mm<sup>2</sup> are adequate for measuring diffusion in the human brain.<sup>32,33</sup> They produce good agreement with six-point estimates.<sup>34</sup> However, it may be possible to improve the quality of data by increasing the number of  $b$  values,<sup>31</sup> though this requires a longer scan time.

## MAGNETIC RESONANCE SPECTROSCOPY

The magnetic environment experienced by each MR sensitive nucleus is different. Although all nuclei are dominated by the  $B_0$  and applied  $B_1$  field, they will also experience a local magnetic force due to the magnetic fields of the electrons within their immediate chemical environment. Thus, the degree of shielding or enhancement of the local magnetic field by electron currents depends on the exact electronic environment, a function of the chemical structure. Different chemical environments will produce different nuclear resonant frequencies. This gives rise to the phenomenon of chemical shift, whereby the MR frequency spectrum consists of nuclei, which resonate at different frequencies.<sup>5</sup> The frequency depends on the exact magnetic field strength, and so is usually expressed in dimensionless units (parts per million, ppm), by reference to a specific reference point; in <sup>1</sup>H MR spectroscopy, this is usually water at 4.7 ppm. <sup>1</sup>H and <sup>31</sup>P are the main nuclei investigated in clinical MRS, but <sup>13</sup>C, <sup>23</sup>Na, and <sup>19</sup>F are also amenable to MRS investigation, if appropriate coils are available to overcome the problem of low signal-to-noise ratio in these isotopes. Peaks in the MR spectra are also called resonances. Some metabolites may be split into two (doublet) or more subpeaks. The area beneath the peak represents the concentration of the metabolite. Absolute quantification of metabolites is theoretically possible, but can be difficult to achieve accurately owing to factors including  $T_1$  and  $T_2$  effects.<sup>35</sup> Therefore, results are usually reported as metabolite ratios to a stable metabolite occurring naturally in tissue, such as creatine.

## DATA ACQUISITION

The two main clinical techniques for in vivo MRS are single-voxel spectroscopy and chemical shift imaging.

Single-voxel spectroscopy uses gradients to define a voxel of interest within an organ. The size of the voxel is predefined by the user and is the only source of signal. To improve the signal-to-noise ratio in smaller voxels, the number of signal averages acquired may be increased, requiring increased scanning time. Chemical shift imaging (CSI) acquires spectra from a matrix of voxels. In principle, this can be done in all three directions, but in practice, it is usually done in one plane, hence the name, 2D-single slice CSI. Single-voxel spectroscopy has the advantage of greater signal-to-noise, whereas CSI allows wider anatomical coverage.

### SINGLE-VOXEL SPECTROSCOPY

The height of the MRS peaks depends on the metabolite concentration, spectroscopy sequence, TR, and echo time (TE). The ideal scenario is to avoid signal loss due to  $T_1$  relaxation and  $T_2$  decay, and thus the TR should be at least 2000 ms, certainly no less than 1500 ms, and the TE as short as possible, usually 30–35 ms. The TE determines the information acquired, a short TE maximizes the data acquired, but a longer TE attenuates the signal from the unwanted macromolecule resonances, such as lipids.<sup>36</sup>

### MRS SEQUENCES

A number of different MRS sequences have been developed, which differ in pulse sequences and localization methods. Stimulated echo acquisition mode (STEAM) historically used to be the only sequence capable of short echo times.<sup>37</sup> Point-resolved spectroscopy (PRESS) uses a 90 degree pulse followed by two 180 degree pulses. Each pulse has a slice selective gradient on one of the three principle axes, so that protons within the voxel are the only ones to experience all three RF pulses.<sup>38</sup> The signal intensity acquired with PRESS is twice as high as STEAM. Modern equipment and sequences are now able to produce short-echo-time PRESS.<sup>39</sup>

### DATA ANALYSIS

Several issues need to be considered with respect to interpretation of MRS data. A number of experimental factors contribute to the accuracy of the data: hardware (coil characteristics, linearity of receiver, field homogeneity, and homogeneity over the voxel), efficiency of water suppression, and voxel localization, by pulse sequence and the analysis technique method used to quantify the data.<sup>40</sup> One must also consider the physical characteristics of the tissues under investigation and the analysis technique employed. For example, water concentration varies between different tissue classes, such as gray and white

matter in the brain. Therefore, if water is used as an internal reference for quantification, calculations of metabolite concentrations may be affected if the tissue composition of a voxel cannot be accurately determined.<sup>41</sup> Different software programs exist for analyzing MRS data; identical spectra analyzed by different techniques can produce varying results for metabolite levels.<sup>42</sup> Thus, when spectra are analyzed by different investigators, there may be variability in the metabolite ratios.<sup>40</sup>

### CEREBRAL PROTON SPECTROSCOPY-VISIBLE METABOLITES

The most important visible peaks on the cerebral proton MR spectrum are N-acetyl aspartate (NAA), choline (cho), creatine (Cr) myo-inositol (mI), and the combined glutamine and glutamate peak (Glx); lactate (Lac) may also be visible. At a TE of 30 ms, the NAA resonance is at 2.0 parts per million (ppm), cho at 3.2 ppm, Cr at 3.0 ppm, mI at 3.6 ppm, the Glx complex between 2.1 and 2.5 ppm and the lactate doublet around 1.3 ppm.

**N-acetyl aspartate** is the major peak seen on water suppressed proton spectroscopy, but its exact physiological role is not known.<sup>42</sup> It is regarded as a marker of neuronal dysfunction and neuronal loss and is used clinically in the study of disease progression in multiple sclerosis.<sup>43</sup>

**Choline** is considered to be a marker of membrane activity, since phosphocholines are released during membrane breakdown. The phosphocholines also participate in phospholipid metabolism and osmotic regulation in glial cells. The choline resonance is elevated in a variety of inflammatory and malignant processes, probably representing increased cellularity, gliosis, and membrane degradation due to myelin breakdown.<sup>41,44–46</sup> Decreases in choline resonance have been associated with osmoregulatory changes in hepatic encephalopathy.<sup>47</sup>

**Creatine** is the total peak from creatine and phosphocreatine and is often taken as the internal reference level. It is assumed to be constant in concentration throughout the brain in health and disease.<sup>41</sup> However, it may be that in certain disease states, such as HIV-related dementia, the creatine level may be affected.<sup>48</sup>

**Myo-inositol** is a sugar alcohol involved in the synthesis of phosphoinositides and a cerebral osmolyte involved in cerebral osmoregulatory processes.<sup>49</sup> Elevated levels of myo-inositol have been associated with microglial activation and astrogliosis.<sup>44</sup>

**Glutamine and glutamate** metabolism are interrelated. Astrocytes take up glutamate from the capillaries and combine it with ammonia by the action of glutamine synthetase to produce glutamine. Neurons subsequently take up glutamine and convert it to glutamate, a neurotransmitter, by the action of glutaminase.



## METABOLITE QUANTIFICATION

There are two main methods of expressing the concentration of metabolites in MRS, either as absolute values or ratios. Absolute quantification requires either the use of external reference solutions, “phantoms”, or more commonly utilizing tissue water as an internal reference within the MR scanner.<sup>50</sup> The advantage of absolute quantification is the ability to describe individual metabolite concentrations and variations in disease states. There are, however, a number of technical and methodological issues. If one uses external reference solutions, there is concern regarding  $B_1$  field inhomogeneity in the two disparate regions of interest. Using water as an internal reference, the water content has to be assumed, but this may change in disease states, and focal lesions. Additionally, different tissue classes may have different water contents, for example gray and white matter in the brain.<sup>50</sup> Water constitutes over 70% of brain tissue mass and is thus present at over 10,000 times the concentration of most metabolites (10 mmol/L).<sup>41</sup> Therefore, small errors in the assignment of a value to the absolute water concentration will affect the calculated concentrations of metabolites. With absolute quantification methods, the effects of  $T_1$  and  $T_2$  relaxation on water and metabolite peaks need to be accounted for and additional measurements need to be taken while a subject is in the MR scanner, prolonging examination time. Metabolite ratios work on the presumption that the concentration of creatine is stable in health and disease, which may be incorrect. However, as the comparison being made is at the same time point and within the same region of interest, the error should be dynamic and therefore minimized.

## MRS ANALYSIS

Metabolite peaks are usually calculated by integration or line-fitting of the Fourier transformed signal using proprietary software. Accuracy can be improved by the use of a prior-knowledge based approach, defined as previously obtained information regarding the component characteristics of the spectrum, which are likely to be different between different hardware and acquisition sequences.<sup>51</sup> One such software package that incorporates the prior knowledge methodology is JMRUI, which uses the AMARES algorithm.<sup>51,52</sup> Another advantage of the use of prior knowledge is reduction of user-dependent input, which could otherwise lead to further operator-dependent variability. JMRUI analyses spectra in the time domain. Analysis of spectroscopy data in the time domain, rather than the frequency domain, is advantageous, allowing better coping with artifacts, such as baseline roll and any underlying broad spectral component due to unwanted noise within the data.<sup>53</sup>

## MRI IN THE FUTURE

Although a lot of progress has been made in the cost and therefore availability of MRI, it is expected that the cost of MR scanners will be driven down even more over the coming years, improving accessibility. Investigations, such as MR cholepancreatography and MRI of the liver, pancreas, abdomen, and brain, will become commonplace. Magnetic field strength is also expected to increase with 3 T machines being used routinely in some areas even now; this can be expected to roll out across the country. Higher resolution and tissue contrast will further enhance the importance of MRI in routine diagnosis, decreasing the number of invasive diagnostic procedures, such as endoscopy, performed. To summarize, it is our view that the underlying physical principles of MRI are an important concept for the clinician to appreciate. An accurate understanding of the limitations of the techniques employed will ensure appropriate use.

## SUMMARY OF KEY ISSUES

- The principles of nuclear “spin” and how nuclei react when external magnetic fields are applied to them underpin the functioning mechanism of MRI.
- MR pulses must be applied at a particle’s resonant frequency to generate a free-induction decay and therefore a signal that can be converted into readable data.
- MR gradients are required to localize MR signals in space/tissue. These are generated using multiple radiofrequency coils arranged in different positions in space.
- Parallel imaging utilizes multiple RF coils to reduce scan time.
- 3 T systems are regularly used in the research setting, exhibiting improved signal-to-noise ratio and higher resolution than regular 1.5 T models generally used in clinical practice.
- Magnetization transfer imaging can be used to visualize normally MR-invisible protons bound to macromolecules, allowing indirect measurement of protein/lipid components versus body water.
- Diffusion-weighted imaging allows imaging of the water component of the brain; diffusion tensor imaging allows detailed information of water movement at a microscopic, cellular level.
- Magnetic Resonance Spectroscopy can be used to determine the exact chemical makeup of a sample, performed by single-voxel spectroscopy or chemical shift imaging. Observations made about changes in normal tissue metabolism have clinical relevance.

## CONFLICTS OF INTEREST

The authors have none to declare.

## ACKNOWLEDGEMENTS

All authors acknowledge the support of the National Institute for Health Research Biomedical Research Centre at Imperial College London for infrastructure support. VPBG was supported by grants from the Royal College of Physicians of London, the University of London and the



Trustees of St Mary's Hospital, Paddington. MMEC is supported by a Fellowship from the Sir Halley Stewart Trust (Cambridge, United Kingdom). MMEC and SDT-R hold grants from the United Kingdom Medical Research Council.

## REFERENCES

- Bloch F, Hansen WW, Packard ME. Nuclear induction. *Phys Rev.* 1946;69:127.
- Purcell EM, Torrey HC, Pound RV. Resonance absorption by nuclear magnetic moments in a solid. *Phys Rev.* 1946;69:37–38.
- Hawkes RC, Holland GN, Moore WS, Worthington BS. Nuclear magnetic resonance (NMR) tomography of the brain: a preliminary clinical assessment with demonstration of pathology. *J Comput Assist Tomogr.* 1980;4(5):577–586.
- Smith FW, Hutchison JM, Mallard JR, et al. Oesophageal carcinoma demonstrated by whole-body nuclear magnetic resonance imaging. *Br Med J (Clin Res Ed).* 1981;282(6263):510–512.
- Westbrook C, Roth CK, Talbot J. *MRI in Practice*. 4th edition London: John Wiley & Sons, Inc.; 2011.
- Di Costanzo A, Trojsi F, Tosetti M, et al. High-field proton MRS of human brain. *Eur J Radiol.* 2003;48(2):146–153.
- Soher BJ, Dale BM, Merkle EM. A review of MR physics: 3 T versus 1.5 T. *Magn Reson Imaging Clin N Am.* 2007;15(3):277–290.
- Rovira A, Cordoba J, Sanpedro F, Grive E, Rovira-Gols A, Alonso J. Normalization of T<sub>2</sub> signal abnormalities in hemispheric white matter with liver transplant. *Neurology.* 2002;59(3):335–341.
- Rovira A, Grive E, Pedraza S, Rovira A, Alonso J. Magnetization transfer ratio values and proton MR spectroscopy of normal-appearing cerebral white matter in patients with liver cirrhosis. *Am J Neuroradiol.* 2001;22(6):1137–1142.
- Hajnal JV, Baudouin CJ, Oatridge A, Young IR, Bydder GM. Design and implementation of magnetization transfer pulse sequences for clinical use. *J Comput Assist Tomogr.* 1992;16(1):7–18.
- Wolff SD, Balaban RS. Magnetization transfer contrast (MTC) and tissue water proton relaxation in vivo. *Magn Reson Med.* 1989;10(1):135–144.
- Baird AE, Warach S. Magnetic resonance imaging of acute stroke. *J Cereb Blood Flow Metab.* 1998;18(6):583–609.
- Moseley ME, Kucharczyk J, Mintorovitch J, et al. Diffusion-weighted MR imaging of acute stroke: correlation with T2 weighted and magnetic susceptibility-enhanced MR imaging in cats. *AJNR Am J Neuroradiol.* 1990;11(3):423–429.
- Larsson HB, Thomsen C, Frederiksen J, Stubgaard M, Henriksen O. In vivo magnetic resonance diffusion measurement in the brain of patients with multiple sclerosis. *Magn Reson Imaging.* 1992;10(1):7–12.
- Kono K, Inoue Y, Nakayama K, et al. The role of diffusion-weighted imaging in patients with brain tumors. *AJNR Am J Neuroradiol.* 2001;22(6):1081–1088.
- Stadnik TW, Chaskis C, Michotte A, et al. Diffusion-weighted MR imaging of intracerebral masses: comparison with conventional MR imaging and histologic findings. *AJNR Am J Neuroradiol.* 2001;22(5):969–976.
- Chenevert TL, Brunberg JA, Pipe JG. Anisotropic diffusion in human white matter: demonstration with MR techniques in vivo. *Radiology.* 1990;177(2):401–405.
- Doran M, Hajnal JV, Van Bruggen N, King MD, Young IR, Bydder GM. Normal and abnormal white matter tracts shown by MR imaging using directional diffusion weighted sequences. *J Comput Assist Tomogr.* 1990;14(6):865–873.
- Basser PJ, Mattiello J, LeBihan D. MR diffusion tensor spectroscopy and imaging. *Biophys J.* 1994;66(1):259–267.
- Basser PJ, Jones DK. Diffusion-tensor MRI: theory, experimental design and data analysis—a technical review. *NMR Biomed.* 2002;15(7):456–467.
- Mori S, van Zijl P. 2005, MR tractography using diffusion tensor imaging. In: Gillard J, Waldman A, Barker PB, eds. In: *Clinical MR Neuroimaging* 1st edition Cambridge University Press; 2005:86–98.
- Jones DK. Fundamentals of diffusion MR imaging. In: Gillard J, Waldman A, Barker PB, eds. In: *Clinical MR Neuroimaging* 1st edition Cambridge University Press; 2005:54–85.
- Mori S, Barker PB. Diffusion magnetic resonance imaging: its principle and applications. *Anat Rec.* 1999;257(3):102–109.
- Le Bihan D, Breton E, Lallemand D, Grenier P, Cabanis E, Laval-Jeantet M. MR imaging of intravoxel incoherent motions: application to diffusion and perfusion in neurologic disorders. *Radiology.* 1986;161(2):401–407.
- Beaulieu C. The basis of anisotropic water diffusion in the nervous system—a technical review. *NMR Biomed.* 2002;15(7):435–455.
- Alexander AL, Lee JE, Wu YC, Field AS. Comparison of diffusion tensor imaging measurements at 3.0 T versus 1.5 T with and without parallel imaging. *Neuroimaging Clin N Am.* 2006;16(2):299–309.
- Kuhl CK, Textor J, Gieseke J, et al. Acute and subacute ischemic stroke at high-field-strength (3.0-T) diffusion-weighted MR imaging: intraindividual comparative study. *Radiology.* 2005;234(2):509–516.
- Habermann CR, Gossrau P, Kooijman H, et al. Monitoring of gustatory stimulation of salivary glands by diffusion-weighted MR imaging: comparison of 1.5 T and 3 T. *AJNR Am J Neuroradiol.* 2007;28(8):1547–1551.
- Kuhl CK, Gieseke J, von FM, et al. Sensitivity encoding for diffusion-weighted MR imaging at 3.0 T: intraindividual comparative study. *Radiology.* 2005;234(2):517–526.
- Lee CE, Danielian LE, Thomasson D, Baker EH. Normal regional fractional anisotropy and apparent diffusion coefficient of the brain measured on a 3 T MR scanner. *Neuroradiology.* 2009;51(1):3–9.
- Correia MM, Carpenter TA, Williams GB. Looking for the optimal DTI acquisition scheme given a maximum scan time: are more b-values a waste of time? *Magn Reson Imaging.* 2009;27(2):163–175.
- Jones DK. The effect of gradient sampling schemes on measures derived from diffusion tensor MRI: a Monte Carlo study. *Magn Reson Med.* 2004;51(4):807–815.
- Xing D, Papadakis NG, Huang CL, Lee VM, Carpenter TA, Hall LD. Optimised diffusion-weighting for measurement of apparent diffusion coefficient (ADC) in human brain. *Magn Reson Imaging.* 1997;15(7):771–784.
- Burdette JH, Elster AD, Ricci PE. Calculation of apparent diffusion coefficients (ADCs) in brain using two-point and six-point methods. *J Comput Assist Tomogr.* 1998;22(5):792–794.
- Bottomley PA. The trouble with spectroscopy papers. *Radiology.* 1991;181(2):344–350.
- Lundbom J, Hakkarainen A, Fielding B, et al. Characterizing human adipose tissue lipids by long echo time <sup>1</sup>H-MRS in vivo at 1.5 Tesla: validation by gas chromatography. *NMR Biomed.* 2010;23(5):466–472.
- Matthaei D, Frahm J, Haase A, Merboldt KD, Hanicke W. Multipurpose NMR imaging using stimulated echoes. *Magn Reson Med.* 1986;3(4):554–561.
- Bottomley PA. Spatial localization in NMR spectroscopy in vivo. *Ann N Y Acad Sci.* 1987;508:333–348.
- Klose U. Measurement sequences for single voxel proton MR spectroscopy. *Eur J Radiol.* 2008;67(2):194–201.
- Keevil SF, Barbiroli B, Brooks JC, et al. Absolute metabolite quantification by in vivo NMR spectroscopy: II. A multicentre trial of protocols for in vivo localised proton studies of human brain. *Magn Reson Imaging.* 1998;16(9):1093–1106.

41. Gadian DG. *NMR and its Applications to Living Systems*. 2nd edn Oxford: Oxford University Press; 1995.
42. Birken DL, Oldendorf WH. N-acetyl-L-aspartic acid: a literature review of a compound prominent in  $^1\text{H}$ -NMR spectroscopic studies of brain. *Neurosci Biobehav Rev*. 1989;13(1):23–31.
43. Vion-Dury J, Meyerhoff DJ, Cozzone PJ, Weiner MW. What might be the impact on neurology of the analysis of brain metabolism by in vivo magnetic resonance spectroscopy? *J Neurol*. 1994;241(6):354–371.
44. Bitsch A, Bruhn H, Vougioukas V, et al. Inflammatory CNS demyelination: histopathologic correlation with *in vivo* quantitative proton MR spectroscopy. *AJNR Am J Neuroradiol*. 1999;20(9):1619–1627.
45. Davie CA, Hawkins CP, Barker GJ, et al. Detection of myelin breakdown products by proton magnetic resonance spectroscopy. *Lancet*. 1993;341(8845):630–631.
46. Miller BL. A review of chemical issues in  $^1\text{H}$  NMR spectroscopy: N-acetyl-L-aspartate, creatine and choline. *NMR Biomed*. 1991;4(2):47–52.
47. Bluml S, Zuckerman E, Tan J, Ross BD. Proton-decoupled  $^{31}\text{P}$  magnetic resonance spectroscopy reveals osmotic and metabolic disturbances in human hepatic encephalopathy. *J Neurochem*. 1998;71(4):1564–1576.
48. Chang L, Ernst T, Witt MD, Ames N, Gaiefsky M, Miller E. Relationships among brain metabolites, cognitive function, and viral loads in antiretroviral-naive HIV patients. *Neuroimage*. 2002;17(3):1638–1648.
49. Häussinger D, Laubenberger J, vom DS, et al. Proton magnetic resonance spectroscopy studies on human brain myo-inositol in hypo-osmolarity and hepatic encephalopathy. *Gastroenterology*. 1994;107(5):1475–1480.
50. Kreis R. Issues of spectral quality in clinical  $^1\text{H}$ -magnetic resonance spectroscopy and a gallery of artifacts. *NMR Biomed*. 2004;17(6):361–381.
51. Vanhamme L, van den Boogaart A, Van Huffel S. Improved method for accurate and efficient quantification of MRS data with use of prior knowledge. *J Magn Reson*. 1997;129(1):35–43.
52. Stubbs M, Van den Boogaart A, Bashford CL, et al.  $^{31}\text{P}$ -magnetic resonance spectroscopy studies of nucleated and non-nucleated erythrocytes; time domain data analysis (VARPRO) incorporating prior knowledge can give information on the binding of ADP. *Biochim Biophys Acta*. 1996;1291(2):143–148.
53. Hamilton G, Patel N, Forton DM, Hajnal JV, Taylor-Robinson SD. Prior knowledge for time domain quantification of *in vivo* brain or liver  $^{31}\text{P}$  MR spectra. *NMR Biomed*. 2003;16(3):168–176.